Equationof- State, Shock-Temperature, and Electrical-Conductivity Data of Dense Fluid Nitrogen in the Region of the Dissociative Phase Transition

ARTICLE *in* THE JOURNAL OF CHEMICAL PHYSICS · JANUARY 1991

Impact Factor: 2.95 · DOI: 10.1063/1.459895

Equation-of-state, shock-temperature, and electrical-conductivity data of dense fluid nitrogen in the region of the dissociative phase transition

W. J. Nellis, H. B. Radousky, D. C. Hamilton,[a] A. C. Mitchell, N. C. Holmes, K. B. Christianson,[b] and M. van Thiel
Lawrence Livermore National Laboratory, University of California, Livermore, California 94550

(Received 24 August 1990; accepted 23 October 1990)

The dissociative phase transition of fluid nitrogen at pressures in the range 30–110 GPa (0.3–1.1 Mbar), temperatures in the range 4000–14 000 K, densities up to 3.5 g/cm^3, and internal energies up to 1 MJ/mol was investigated by shock compression. Equation-of-state, shock-temperature, and electrical-conductivity experimental data are presented and analyzed in detail.

I. INTRODUCTION

Nitrogen is one of the most thoroughly investigated materials at high pressures because it is a relatively simple diatomic molecule which undergoes phase transitions in both the fluid and solid phases. One of these transitions is molecular dissociation in the dense, high-temperature fluid.[1,2] Because of its interesting properties at high pressures and temperatures, its cosmological abundance, and its ability to form numerous chemical compounds, nitrogen is of importance to condensed matter physics, planetary interiors, and chemical explosives.

A. Molecular fluid phase

The molecular fluid phase has been studied extensively by the shock compression of liquid nitrogen to obtain equation-of-state (EOS) data.[3-6] The molecular range extends up to about 30 GPa (300 kbar), 2 g/cm^3, and 7000 K on the principal Hugoniot, the single-shock-compression curve starting from liquid density. The pressure–volume (P–V) data to 30 GPa were successfully explained by a theory which scales the spherically symmetric exponential-six pair potential of Ar by critical point parameters, assumes rotational degrees of freedom are fully excited, and assumes that molecular vibrational levels are equally spaced in energy, as in the gas phase, and populated according to a Maxwell–Boltzmann distribution. This theory calculates a P–V curve in excellent agreement with shock data up to about 30 GPa and 7000 K[7] and provides evidence that the N_2 molecule persists to these extreme conditions. The scaled theory also calculates temperatures in good agreement with shock-temperature data in the molecular phase.[2,8]

The excellent agreement between theory and experiment for the equation-of-state and thermal data also means that molecular vibrational equilibrium is achieved in a time of ~ 1 ns, the time resolution of the shock-velocity measurement of the equation-of-state experiments. If vibrational equilibrium were not achieved on the experimental time scale, then more shock-compression energy would be distributed into molecular kinetic energy and the experimental P–V curve would be stiffer than observed.[7] The relaxation time for energy transfer from translational to vibrational degrees of freedom has been calculated to be ~ 0.5 ns for fluid N_2 at conditions comparable to 30 GPa shock pressure,[9] in agreement with the above considerations of the P–V data.

Pulsed coherent anti-stokes Raman scattering (CARS) spectra have been measured for liquid N_2 single shocked up to 19 GPa and double shocked up to 41 GPa.[10,11] These spectra show that the spacings between vibrational levels of N_2 are constant within the uncertainties of the experimental data and consistent with gas-phase values. These data also show that excited vibrational states of N_2 are populated in $\leqslant 10$ ns, an upper bound equal to the duration of the laser pulse used for the Raman scattering experiments.[11]

Anisotropic N_2–N_2 interaction potentials have been derived.[12,13] For dense fluid N_2 the optimal spherical potential is the median of the full anisotropic potential[14] and effective spherical potentials can be found that yield thermodynamic data in good agreement with experiment.[7,15,16] Small Raman shifts in dense fluid molecular nitrogen have been calculated theoretically,[17,18] and are in good agreement with the Raman spectra of shocked liquid N_2.

B. Molecular dissociation

Nitrogen undergoes a dissociative phase transition in the fluid phase above 30 GPa, 2 g/cm^3, and 7000 K on the principal Hugoniot. This transition was first observed as an increase in the compressibility (softening of the P–V curve) above 30 GPa followed by a decrease in compresibility (stiffening of the P–V curve) above 60 GPa.[1,5] The observation of the phase change was made possible by the use of a two-stage light-gas gun to generate strong shock waves. The two-stage gun has a maximum velocity of 8 km/s, while the planar explosive systems used previously have a maximum velocity of 5 km/s. The higher velocity produces about twice the shock pressure on impact with a target specimen.

Dissociation was identified as the nature of the phase transition[1] by the comparison of the principal Hugoniots of N_2 and isoelectronic CO with the theory for the molecular phase. Deviation of the P–V data of CO from the theory was

[a] Present address: Boeing Aerospace & Electronics, Seattle, WA.
[b] Present address: Department of Physics, Caltech, Pasadena, CA.

 0021-9606/91/032244-14$03.00

attributed to molecular decomposition because carbon compounds are generally known to decompose at sufficiently high pressures and temperatures. The main decomposition product of isoelectronic N_2 is expected to be simply atomic N because the temperatures are above 7000 K and the formation of other pure nitrogen compounds with bonds stronger than the triple bond of N_2 is unlikely at such high temperatures. Also, the phase transition region is close to a region of density in which theory indicates that monatomic solid nitrogen might be metastable at 0 K.[1,19] Thus, high shock temperatures could be expected to drive the transition to a denser monatomic phase.

To obtain more experimental information about the nature of the phase transition double-shock EOS points were measured, which included the first observation of double-shock states above the principal Hugoniot in P–V space.[1] These data show that $(\partial E/\partial P)_v < 0$ and the average Grüneisen parameter $\gamma = V(\Delta P/\Delta E)_v < 0$, since specific internal energies of the double-shock EOS points above the Hugoniot are lower than for states on the Hugoniot at the same respective volumes. In addition, $(\partial E/\partial P)_v < 0$ implies that $(\partial T/\partial P)_v < 0$, since heat capacity is positive.[1] All these negative thermodynamic derivatives are indicative of a phase transition near 2.5 g/cm^3 and 8000 K.

The unusual thermal properties derived from the EOS data led us to measure shock temperatures of nitrogen.[2] Single-shock temperatures vs volume show a thermal softening above 30 GPa, analogous to the P–V data. Double-shock temperature experiments verify that $(\partial T/\partial P)_v < 0$, as predicted from the EOS data and provide evidence for crossing isotherms because the temperatures of nearly the same P–V states obtained by single and double shock differ by a factor of 2.

Double-shock temperature experiments also showed that the temperature of a second-shock state, achieved by reflecting an incident shock off a transparent window, could be lower than the temperature of the incident first-shock state. We call this phenomenon shock-induced cooling.[2] It was an unexpected observation because shock compression normally heats material. The cooling indicates that so much internal energy is absorbed in the dissociative phase transition at the higher pressure and density of the double-shock state that the temperature of this state is actually lower than that of the first-shock state.

Several theoretical models have been developed for the dissociation of dense fluid nitrogen. Ross uses his N_2–N_2 pair potential $\phi_{N_2\text{-}N_2}$ to construct atom–atom and atom–molecule potentials as $\phi_{N_2\text{-}N} = 1/2\phi_{N_2\text{-}N_2}$ and $\phi_{N\text{-}N} = 1/2\phi_{N_2\text{-}N}$. The dissociation energy is taken as the free molecule value, 9.9 eV, for volumes down to 20 cm^3/mol. At smaller volumes the effective dissociation energy is decreased quadratically with volume to match the principal Hugoniot data. Vibrational levels of the free N_2 molecule are used. Excited electronic levels for N_2 and N are also taken as for the free molecule and atom, respectively. The free energy of mixing N_2 and N is included in the total free energy.[20,21] Hamilton and Ree performed chemical equilibrium calculations using the same N_2–N_2 potential. The N–N and N_2–N potentials are determined from these calculations using mixing rules used to calculate an effective one-component fluid. This model takes into account the very dissimilar length scales of the N_2–N_2, N–N, and N_2–N interactions.[22] One result of their calculations is that the N_2–N_2 and N–N potentials can be used to estimate the relative sizes of the nitrogen molecule and atom. That is, by approximating the particle diameter as the distance at which the respective potentials are zero, the volume of the N_2 molecule is about twice that of 2 N atoms. Thus, high shock temperatures are expected to drive dissociation to a more dense phase as a mechanism to accomodate high densities. Kerley and Switendick also used a chemical equilibrium model and compute the equation of state of the ideal mixture from equations of state of the pure molecular and atomic fluids. The softening in the Hugoniot is attributed to the higher density of the monatomic phase and to the fact that dissociation absorbs internal energy and lowers the temperature of the system.[23]

Electrical conductivities of shocked liquid nitrogen were measured in the range 19–61 GPa and 4000–12 000 K. Electrons are probably the dominant carriers by virtue of their high mobility relative to ions. Above 30 GPa the conduction electrons are ionized primarily from dissociated N atoms because excited electronic states of the N atoms are at significantly lower energies than for the N_2 molecule.[2]

C. Melting

The melting curve of N_2 has been measured to 18 GPa and 900 K in a diamond-anvil cell.[24] Theoretical analysis of the experimental data shows that the melting of N_2 is influenced strongly by librational motion in the dense solid. The lowest published shock-temperature measurement of 2000 K at 10.6 GPa[8] is well above the melting temperature of 600 K at this pressure. Linear extrapolation of the melt line from 18 to 30 GPa, which probably overestimates the melting temperature, gives a value of 1300 K. Thus, the temperature of the softening of the Hugoniot curve at 30 GPa and 7000 K is more than 5 times the melting temperature. Hence, the phase transition in nitrogen at high shock pressures and temperatures is definitely well into the fluid phase and not the result of the formation of dense polymeric phases, for example.

D. Solid molecular phases

The observation of a phase transition above 30 GPa in shock-compressed liquid nitrogen led to a theoretical prediction that at 0 K solid N_2 might transform to a monatomic phase at a pressure possibly below 100 GPa.[25] Raman-scattering experiments up to about 150 GPa at 300 K in a diamond-anvil cell showed that solid N_2 retains its diatomic nature up to this pressure, although three transitions to new structures are observed.[26,27] The fact that N_2 dissociates in the dynamic experiments and not in the static ones shows that high shock temperatures drive this transition.

The 300 K static-compression P–V curve of solid N_2 was measured from 5 to 10 GPa.[28] The phase diagram of solid N_2 has been mapped up to 52 GPa by Raman[29,30] and Brillouin scattering.[31]

The purpose of this paper is to present the experimental details, data analysis, and numerical tabulations of our equation-of-state, shock-temperature, and electrical-conductivity measurements of nitrogen[1,2] in the region of the dissociative phase transition.

II. EQUATION-OF-STATE MEASUREMENTS

A. Experiments

Strong planar shock waves were generated by the impact of a metal plate onto a cryogenic specimen holder. The impactor plates were accelerated to velocities of 4–8 km/s by means of a two-stage light-gas gun described previously.[32,33] The specimen holders and experimental techniques for single- and double-shock equation-of-state experiments for cryogenic liquid specimens were also described previously.[5,34] Briefly, the specimen holder for the double-shock experiments consists of an Al wall, a liquid nitrogen specimen, and a Cu anvil. A metal impactor strikes the Al and generates a shock wave which is transmitted into the nitrogen. When the shock reaches the Cu anvil, it increases in amplitude and reflects back into the nitrogen, thus double shocking the nitrogen specimen. The transmitted shock traverses the Cu anvil.

The design of the equation-of-state experiments is based on the Rankine–Hugoniot equations, which are derived from the conservation of mass, momentum, and energy across the front of a shock wave. The equations are

$$P - P_0 = \rho_0 (u_s - u_0)(u_p - u_0), \tag{1a}$$

$$V = V_0 [1 - (u_p - u_0)/(u_s - u_0)], \tag{1b}$$

and

$$E - E_0 = 1/2(P + P_0)(V_0 - V), \tag{1c}$$

where P_0, ρ_0, E_0, and u_0 are, respectively, the initial pressure, density, specific internal energy, and velocity of the material; $V_0 = 1/\rho_0$ is the initial specific volume; P, V, and E are, respectively, the final shock pressure, specific volume, and specific internal energy; u_s is the velocity of the shock wave; and u_p is the mass velocity behind the shock front. For the first shock the initial velocity of the material is $u_0 = 0$. P_0 and T_0 were measured. V_0 and E_0 were obtained from the known equation of state of liquid N_2 along the saturation curve near 77 K.[35] For the single-shock Hugoniot point at 83 GPa, impact velocity u_I and shock velocity u_s were measured and mass velocity u_p was determined by the shock impedance matching method. For double-shock experiments the initial states [with zero subscripts in Eqs. (1a)–(1c)] are the first-shock states and the second-shock states are then the unsubscripted variables in Eqs. (1a)–(1c).

Error analysis[34,36] has shown that in our double-shock experiments it is more accurate to determine the first-shock state by shock impedance matching rather than by measuring shock velocity in the specimen. The shock impedance matching method uses the measurement of impact velocity u_I, which is the most accurate measurement we make (to within $\pm 0.1\%$ as opposed to typically $\pm 1\%$ for u_s), and fits to Hugoniot data for the metal impactor, Al wall, and liquid nitrogen. Each fit in effect averages over many data points and is more accurate than any one measurement. The systematic error in using Hugoniot fits is calculated and small. Thus, for the double-shock equation-of-state experiments u_I was measured to determine the first-shock state and u_s was measured in a Cu anvil. The second-shock state was then determined from the Hugoniot of Cu initially at 77 K, obtained by small correction to the Hugoniot of Cu initially at 300 K by using a Grüneisen equation of state.[5] The Hugoniot equations of state used for shock impedance matching are listed in Table I. The strength of Al is negligibly small at the pressures in these experiments[37] and was neglected.

In shock impedance matching, the same release isentrope for the Al wall, obtained by corrections to the "mirror reflection" of the Al Hugoniot, was used as previously.[5] However, the correction was incorrectly stated previously. The coefficients listed before[5] are for the *fractional* correction and Eq. (8) of Ref. 5 should read

$$(u_p - u_{pH})/u_{pH} = B_0 + B_1 (u_{pH} - u_{pw}) + B_2 (u_{pH} - u_{pw})^2, \tag{2}$$

where u_p is the mass velocity of Al and liquid on release of Al into the liquid specimen, u_{pH} is the mass velocity obtained by approximating the Al release isentrope by the Al Hugoniot reflected about a vertical in $P - u_p$ space through the impact shock state in the Al wall, u_{pw} is the mass velocity of the impact shock state in Al, and $B_0 = -0.001\,096$ μs/cm, $B_1 = 0.056\,71$ μs/cm, and $B_2 = 0.1276$ (μs/cm)^2, as previously. Equation (2) is the form used in the analyses of these and all our previous liquid experiments.

It was desirable to extend the single-shock Hugoniot to the highest possible pressure in order to determine the volume range in which double-shock points lie above the Hugoniot. To extend our highest pressure Hugoniot point from 64 to 83 GPa it was necessary to decrease projectile mass in order to increase maximum impact velocity from 6.8 to 7.8 km/s. Thus, diameter and thickness of the Ta impactor plate were decreased from 25 and 1.5 mm to 20 and 1.0 mm, respectively. In turn, the thickness of the Al container wall and of the liquid N_2 shock transit distance were both decreased to 1.5 mm from 2.0 and 2.3 mm, respectively. The radii of our standard detector array for liquid specimens were reduced from 18 and 10 mm to 10 and 6 mm for this shot, LN213.

TABLE I. Coefficient C and S, where $u_s = C + Su_p$, for Hugoniots of materials used for impactors, walls, and anvils.

Material	T_0 (K)	C (cm/μs)	S
Al	300	0.5386	1.339
Al	80	0.5420	1.334
Cu	300	0.3933	1.500
Cu	80	0.3960	1.500
Ta	300	0.3293	1.307
Al_2O_3	80	0.876	0.957
LiF	300	0.509	1.405

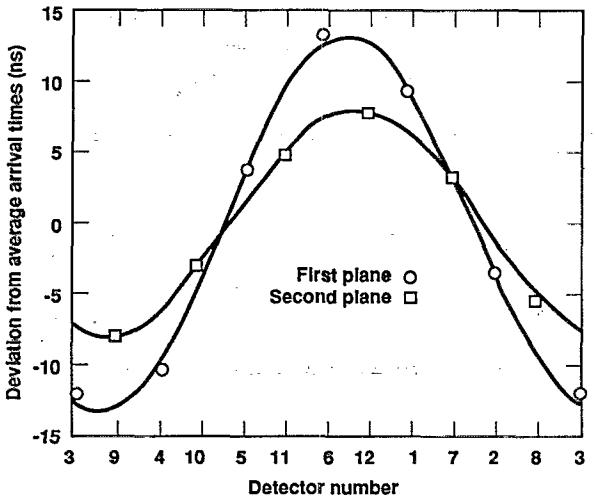

FIG. 1. Shock arrival time, relative to average arrival time on each of two planes, vs detector number for two circular detector arrays on double-shock experiment LN212. Standard deviations from fits are few 0.1 ns. First-plane detectors are in liquid N_2; second-plane detectors are pressed against Cu anvil (Ref. 34). Locations of detector numbers are illustrated in Ref. 5.

We performed two double-shock experiments at 65 GPa, one with a relatively thin liquid nitrogen (LN_2) layer and a relatively thick Cu anvil and the other with a relatively thick LN_2 layer and a relatively thin Cu anvil. The data for shots LN27 and LN211 agree within the experimental uncertainties and both lie above the Hugoniot. These results show that the data were not affected by shock reverberations behind the leading shock, a conclusion reinforced by computer simulations of the experiments discussed below. The double-shock point that lies highest above the Hugoniot, shot LN212, is also our most accurate double-shock experiment. The arrival-time data for the two circular detector arrays[5] for this shot are plotted in Fig. 1 to illustrate the small standard deviations for the fits to these arrival times.

B. Results

Table II lists the new single-shock Hugoniot point for nitrogen. Table III lists the experimental parameters for the double-shock Hugoniot experiments. Table IV lists the double-shock Hugoniot data.

Principal Hugoniot data for nitrogen shocked from the liquid near 77 K are plotted in Fig. 2 as shock velocity vs mass velocity. The point at highest velocity is our new one. The $u_s - u_p$ data from Refs. 3 and 5 and our new point are fitted, in the range $0.35 < u_p < 0.87$ cm/μs, by an equation cubic in u_p:

$$u_s = C + \sum_{n=1}^{3} S_n u_p^n , \tag{3}$$

where $C = -0.480\,852\,2$ cm/μs, $S_1 = 5.041\,352$, $S_2 = -6.542\,562$ (cm/μs)$^{-1}$ and $S_3 = 3.401\,672$ (cm/μs)$^{-2}$. The highest pressure point of Ref. 3 was corrected using Eq. (2), since the original data analysis used the mirror reflection method.[3] In the range $0.117 < u_p < 0.436$ cm/μs the data fit the linear relation $u_s = 0.1572 + 1.365\,u_p$.[5] The solid curve of Fig. 2 is comprised of the cubic fit above 0.35 cm/μs (3.5 km/s) and the linear fit at lower mass velocities. The data of Ref. 6 were not used to determine the fitting parameters, because initial specimen densities were 5% smaller than the other data. However, the data of Ref. 6 are in excellent agreement with the fit.

Three of the double shock points (LN27, LN211, and LN212) lie above the principal Hugoniot in P–V space and are shown plotted in Fig. 3. Double-shock data at lower pressures have also been reported.[6] The double-shock data and the fit for the principal Hugoniot were used to calculate average Grüneisen parameter γ from

$$\gamma = V\left(\frac{\Delta P}{\Delta E}\right)_V . \tag{4}$$

The results are plotted in Fig. 4 and listed in Table V as γ vs molar volume. The uncertainties are caused by the uncertainties in the double-shock equation-of-state points and the sensitive variation of pressure and energy with volume along the principal Hugoniot. The specific internal energies of the double-shock points above the Hugoniot are lower than for the states on the Hugoniot at the same volumes, resulting in negative γ's.

C. Computational simulation of experiments

Hydrodynamic computer simulations were performed to verify that shock reverberations in the nitrogen specimen did not affect the double-shock results. These calculations were performed using the one-dimensional KOVEC code in planar symmetry.[38] Measured impactor velocities and material thicknesses were used. For all materials Grüneisen equations of state of the following form were used in the calculations:

TABLE II. Hugoniot data point for liquid N_2. Initial density of Ta impactor was 16.67 g/cm^3 and of Al baseplate 2.732 g/cm^3 at 77 K. Molar volume is calculated per mole of N_2.

Shot	u_f (km/s)	T_0 (K)	ρ_0 (g/cm^3)	u_s (km/s)	u_p (km/s)	P (GPa)[a]	V (cm^3/mol)	E (MJ/mol)
LN_{213}	7.822	78.25	0.8044	11.83 ± 0.12	8.630 ± 0.047	82.13 ± 1.11	9.419 ± 0.341	1.043 ± 0.012

[a] 1 GPa = 10 kbar.

TABLE III. Experimental parameters for double-shock equation-of-state experiments for liquid N_2. All impactors were Al or Al alloy 1100. Average initial density of Al alloy 1100 baseplates was 2.739 g/cm^3 at 77 K. Impactors were 3.0 mm thick and baseplates were 2.0 mm thick. ρ_{0I} is initial impactor density, u_I is impactor velocity, T_0 is initial specimen temperature, ρ_0 is initial specimen density, ΔX_L is thickness of liquid N_2, ρ_{0An} is initial density of Cu anvil at 77 K, ΔX_{An} is anvil thickness at 77 K, and u_{sAn} is shock velocity in anvil.

Shot	ρ_{0I} (g/cm^3)	u_I (km/s)	T_0 (K)	ρ_0 (g/cm^3)	ΔX_L (mm)	ρ_{0An} (g/cm^3)	ΔX_{An} (mm)	u_{sAn} (km/s)
LN27	2.699	4.741	77.32	0.8088	1.90	8.995	1.553	5.816 ± 0.058
LN211	2.713	4.842	77.3	0.809	2.22	8.982	1.043	5.840 ± 0.076
LN212	2.713	5.500	77.3	0.809	2.19	9.002	1.046	6.208 ± 0.045
LN210	2.716	6.078	77.52	0.8078	2.30	8.980	1.032	6.228 ± 0.066
LN28	2.715	7.167	77.31	0.8088	2.50	8.994	1.142	6.738 ± 0.088

TABLE IV. First-shock and second-shock states for double-shock equation-of-state experiments for liquid N_2. First-shock state was obtained by shock impedance matching. Average initial molar volume was 34.64 cm^3/mol. Molar energies and volumes are calculated per mole of N_2.

Shot	u_{p1} (km/s)	P_1 (GPa)[a]	V_1 (cm^3/mol)	$E_1 - E_0$ (kJ/mol)	u_{p2} (km/s)	P_2 (GPa)[a]	V_2 (cm^3/mol)	$E_2 - E_0$ (kJ/mol)
LN27	3.707 ± 0.03	19.89 ± 0.31	15.28 ± 0.06	192.5 ± 3.2	1.237 ± 0.055	64.73 ± 3.51	11.47 ± 0.61	353.7 ± 21.0
LN211	3.784 ± 0.031	20.63 ± 0.32	15.18 ± 0.06	200.6 ± 3.3	1.253 ± 0.066	65.74 ± 4.35	11.20 ± 0.74	372.3 ± 25.2
LN212	4.253 ± 0.034	25.38 ± 0.38	14.66 ± 0.06	253.4 ± 4.0	1.499 ± 0.046	83.75 ± 3.16	11.02 ± 0.45	452.1 ± 21.3
LN210	4.669 ± 0.034	29.76 ± 0.39	14.16 ± 0.07	305.3 ± 4.5	1.512 ± 0.060	84.56 ± 4.25	9.07 ± 0.76	596.4 ± 34.8
LN28	5.455 ± 0.039	38.61 ± 0.49	13.04 ± 0.07	416.8 ± 6.0	1.852 ± 0.075	112.2 ± 6.0	8.10 ± 0.78	789.4 ± 46.3

[a] 1 GPa = 10 kbar.

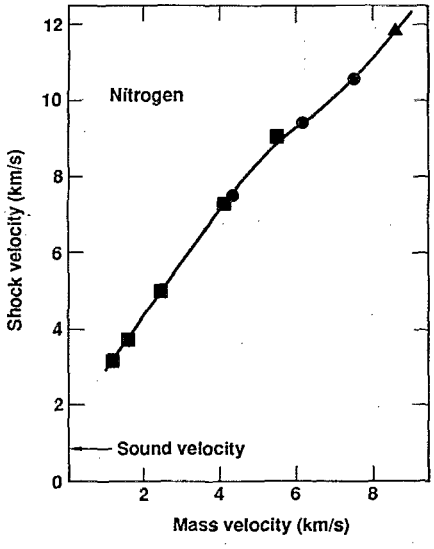

FIG. 2. Shock velocity vs mass velocity for shocked liquid N_2. Squares are from Ref. 3; circles are from Ref. 5; triangle is from this work.

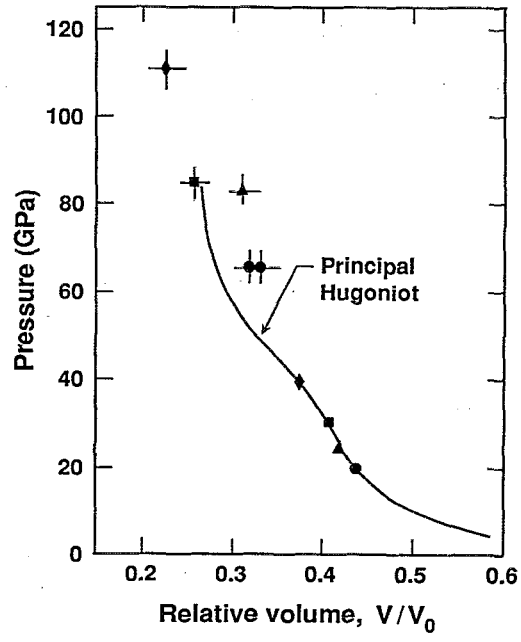

FIG. 3. Double-shock data points and fit to principal Hugoniot data of Fig. 2, plotted as shock pressure vs relative volume. Symbols without error bars are first-shock states and symbols with error bars are corresponding second-shock states (100 GPa = 1 Mbar).

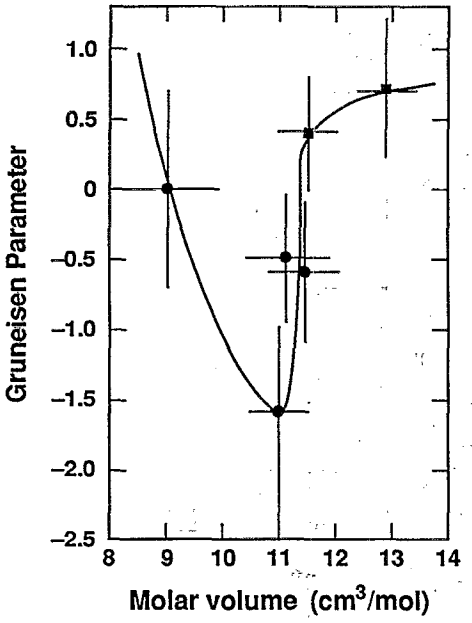

FIG. 4. Average Grüneisen parameter vs molar volume of N_2.

$$P = \frac{\rho_0 D^2 \mu(\mu+1)(1-\frac{1}{2}\gamma\mu)}{\{1-(A_1-1)\mu - A_2[\mu^2/(\mu+1)] - A_3[\mu^3/(\mu+1)^2]\}^2} + \frac{\gamma}{V}E, \quad (5)$$

where $\mu = (\rho/\rho_0 - 1)$, and the coefficients are determined by fits of $u_s - u_p$ data to

$$u_s = D + A_1 u_p + A_2 \frac{u_p^2}{u_s} + A_3 \frac{u_p^3}{u_s^2}. \quad (6)$$

For nitrogen $D = 0.010\,970$ cm/μs, $A_1 = 4.459\,461$, $A_2 = -6.730\,653$, and $A_3 = 3.398\,276$, and Eq. (5) is valid for $V > 10\,\text{cm}^3/\text{mol}$. The form of the Grüneisen parameter in the code is $\gamma = (\gamma_0 + a\mu)/(\mu+1)$. The form of Eq. (6) to represent the Hugoniot as the reference curve of the Grüneisen model leads to the simple algebraic form of Eq. (5).[39]

TABLE V. Average Grüneisen parameters calculated using principal Hugoniot and double-shock equation-of-state data.

V (cm³/mol N_2)	Grüneisen parameter
13.0 ± 0.5	0.7 ± 0.5[a]
11.6 ± 0.5	0.4 ± 0.3[a]
11.5 ± 0.6	-0.6 ± 0.5
11.2 ± 0.7	-0.5 ± 0.45
11.0 ± 0.5	$-1.6^{+0.6}_{-0.9}$
9.1 ± 0.8	0.0 ± 0.7

[a] Double-shock data from Ref. 6.

This is very useful for cases like nitrogen where more than linear terms are required to fit $u_s - u_p$ data. Because the available form for γ cannot generally describe the $\gamma(V)$ of Fig. 4, a constant negative $\gamma(=\gamma_0 = a)$ was used; its value was chosen to produce the measured shock velocity (pressure) in the Cu anvil. These γ values were within the uncertainties shown in Fig. 4. This approach insures that the correct first-shock and second-shock states are obtained in the calculation, which in turn achieves the correct calculated nitrogen compressions and thicknesses. Calculated pressure as a function of distance through the specimen holder is shown in Fig. 5 for shots LN211 and LN212. These profiles are for times just prior to shock arrival at the rear surface of the Cu anvil; that is, at the end of the experiment. These calculations show constant shock amplitudes in the Cu

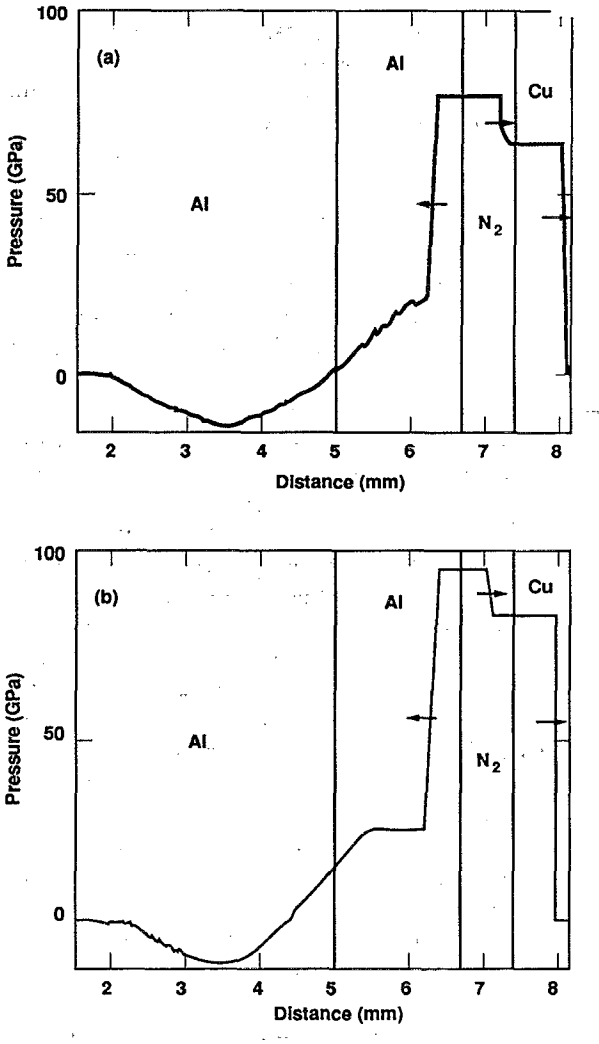

FIG. 5. Calculated pressure along axis of double-shock experiments (a) LN211 and (b) LN212. First Al layer on left is impactor; second Al layer is baseplate; N_2 is specimen; Cu is anvil. Shock velocities in anvil were measured; data for LN212 is shown in Fig. 1. These plots show that the leading steady waves have traversed Cu anvils unaffected by reverberations in N_2 specimens.

anvils extending back into the nitrogen and indicate that the shock velocity measurements in the anvils were unaffected by shock reverberations.

III. SHOCK-TEMPERATURE MEASUREMENTS

A. Experiments

The EOS experiments give P–V–E data points. Temperature must be measured separately. For transparent materials, such as liquid N_2, single-shock temperature is measured from the spectral radiance of light emitted from an opaque shock front as it travels through the material. Light emitted from the shock-compressed and heated portion of the specimen passes through the transparent unshocked portion, through a window, and then to a pyrometer and spectrometer.[40] Shock fronts travel typically at velocities of 10 km/s, which means a few 100 ns are available for the measurements. In double-shock temperature experiments spectral radiance is also measured after the shock in the liquid reflects off a denser window, further shock compressing the specimen to a higher pressure, density, and internal energy. Light emitted from double-shocked nitrogen now passes through the window, which is also shocked and must remain transparent at the high shock pressure of the experiment. The specific P–V–E single- and double-shock states achieved are determined from a measurement of impact velocity, the known P–V–E equation of state of all materials (metal impactor, Al wall, nitrogen, and window), and shock-impedance matching, as discussed below.

The cryogenic specimen holder is illustrated in Fig. 6. It is an adaptation of the one used for EOS experiments for cryogenic liquids.[5] For temperature measurements a window is inserted to permit thermal radiation to exit, rather than an array of shock-arrival-time detectors. Three shock-arrival-time detectors are inserted to provide reference times for triggering the optical diagnostic system. Window materials were Al_2O_3, which remains transparent to 100 GPa,[41] and LiF, which remains transparent to 160 GPa.[42] The pyrometer consisted of up to six photomultiplier (PM) tubes with narrow-band filters placed in front to measure time-resolved intensities at several wavelengths. The filters had a bandpass of 10 nm and were centered, for example, at 310, 370, 450, 546, 598, and 650 nm, although other channels were also used. The spectrometer consisted of two 1000-channel Tracor Northern[43] linear intensified diode arrays mounted on 0.25 m spectrographs. These were used to measure time-integrated emission from 300 to 700 nm over a gated 50 ns time interval. One detector was timed to record the emission spectrum when the first shock reached the center of the sample, while the other detector was timed to record the second-shock spectrum when the shock reached the center of the window/anvil.

Light emitted from the specimen holder (Fig. 6) was sent to the pyrometer by a turning mirror located behind the specimen holder which deflected the light through a window in the wall of the target chamber of the two-stage gun. Light was then distributed to the various PM tubes by a set of beam splitters and dichroic filters. Measured voltages were converted to optical intensities by using a tungsten helicoil lamp

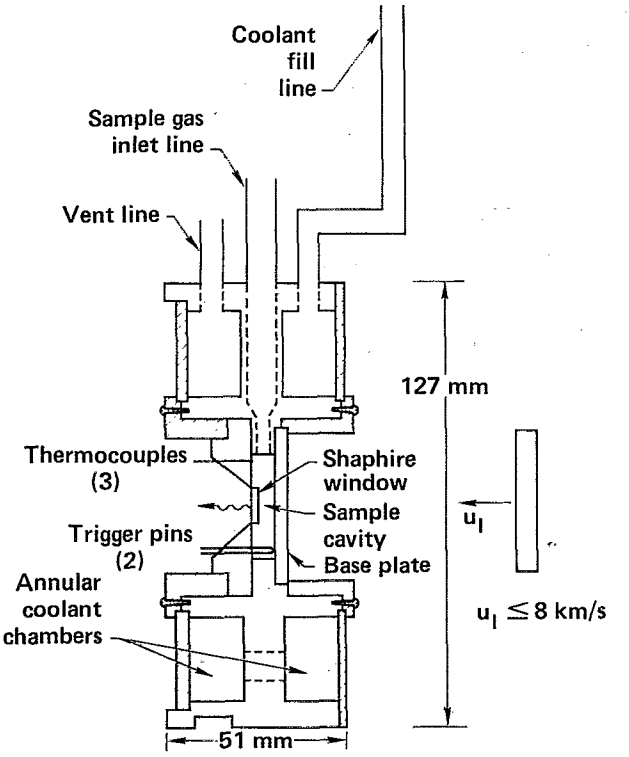

FIG. 6. Cryogenic specimen holder for shock-temperature experiments.

source with a calibrated spectral radiance. The voltage is assumed to be linearly proportional to the optical intensity. The calibration source was placed into the target chamber at the location of the specimen holder prior to each shot, so that light from the calibration source passed through the optical system in a manner identical to the shot configuration.[40] Voltages were measured with model 7103 and 7903 Tektronix[43] oscilloscopes. Oscillograms showing shock-induced cooling have been published elsewhere.[2,21]

Intensity vs wavelength can be measured from 250 to 750 nm with this instrument. The ability to collect data in the ultraviolet (UV) is very important for measurements above about 6000 K. As temperature increases, the peak of the Planck function moves toward shorter wavelengths. As a rough criteria, one wants to measure the spectrum down to the wavelength of the peak in the spectrum. From Wien's law, a temperature of 6500 K corresponds to a peak at 450 nm, which is the lower limit of a visible-range pyrometer. For a UV pyrometer, measuring to 254 nm corresponds to a peak for a 11400 K blackbody curve. The highest temperature measured was 14500 K. To calibrate intensity vs wavelength in the UV, oscilloscopes with mV voltage sensitivity were used for the PM tubes.

To determine temperature the measured spectral intensities were fitted to a graybody Planck function

$$N(\lambda) = \frac{\epsilon C_1}{\lambda^5} (e^{C_2/\lambda T} - 1)^{-1}, \tag{7}$$

where $N(\lambda)$ is the measured intensity at wavelength λ, ϵ is the emissivity assumed to be a constant, T is the temperature, $C_1 = 1.19\times10^{-16}$ W/m^2/sr, and $C_2 = 0.0144$ m K. The uncertainties in the temperatures were calculated by varying sequentially the intensity at each wavelength by the estimated uncertainty in each measured intensity. The absolute values of the deviations between the best-fit temperature and the temperatures obtained by varying the spectral intensities one at a time were then summed to obtain a conservative estimate of the total uncertainty. In cases where the data scatter from the fit is larger than the estimated errors for the individual points, the uncertainty in intensity is taken as the difference between the measured value and the fit value. The larger of the uncertainties calculated in these two ways is taken as the uncertainty in shock temperature.

Intensities vs wavelength are plotted for some representative shots ranging in temperature from 4300 to 12000 K in Fig. 7. The plots show data from the PM tubes, the linear diode arrays, and the fitted curves. The data from the spectrograph systems are smooth and show no evidence of line emission.

The speed of sound at one point in the middle of the phase transition region was measured to estimate the effect of radial edge release and to estimate the value of thermal conductivity. The experiment involves observation of the time at which the longitudinal release wave overtakes the first shock in the liquid nitrogen specimen. For this experiment a thin Cu impactor was used and the arrival of the release is observed by the onset of a decrease in emission intensity in the PM oscillograms. The wave analysis used Grüneisen equations of state for the Cu impactor and Al wall and will be described in a future publication. However, a sound speed of 6.2 km/s was measured on the Hugoniot at 52.6 GPa and 11.1 cm^3/mol. This value permits calculation of the angle of radial edge release from the shock direction;[44] the value obtained is 29°. The Hugoniot EOS experiments were designed to be unaffected by an angle of about 60° and, thus, are unaffected by the radial edge effect.

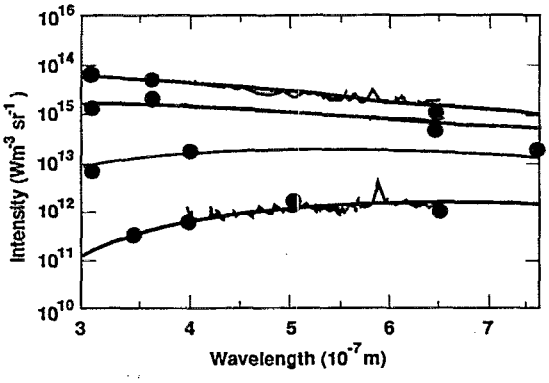

FIG. 7. Spectral radiances for experiments LNT03, LNT02, LNT01, and LNT06, respectively, in decreasing order of intensity. Circles are photomultiplier data points. Solid smooth curves are fits with temperatures and emissivities listed in Table VI. Wiggly curves are measured emission spectra.

B. Shock-impedance matching

The pressures and specific volumes for the single- and double-shock temperature data were obtained from the measured impactor velocities, the known shock-wave equations of state of the materials, and shock-impedance matching. The first-shock states were determined as described previously.[5] The cubic $u_s - u_p$ relation of Eq. (3) resulted in a quartic equation in u_p, rather than the usual quadratic one, in matching the nitrogen Hugoniot with the release isentrope of Al. This quartic equation was solved numerically. The correction to obtain the Al release isentrope from the mirror reflection of the Hugoniot was calculated with Eq. (2).

To obtain the pressures and specific volumes of the double-shock states, an equation of state for nitrogen must be used which takes into proper account the negative $\gamma(V)$ of Fig. 4. Since the common method of approximating a double-shock Hugoniot by the mirror reflection of the principal Hugoniot is of unknown validity in the region of negative $\gamma(V)$, a Grüneisen equation of state was used with the Hugoniot as the reference curve and the $\gamma(V)$ of Fig. 4. This equation is normalized to the single-and double-shock EOS data. Thus, double-shock Hugoniots of nitrogen starting from the respective experimental first-shock states were calculated using Eq. (5) and shock-impedance matched with the Hugoniot of the window material. Equation (5) is substituted into Eq. (1c) to restrict it to double-shock states and solved for E_2:

$$E_2 = \frac{E_1 + \frac{1}{2}[\,f(\mu_2) + P_1\,](V_1 - V_2)}{1 - \frac{1}{2}(\gamma/V_2)(V_1 - V_2)}, \tag{8}$$

where subscript 1 refers to the first-shock state, 2 refers to the double-shock state, $\gamma(V)$ is shown in Fig. 4, and $f(\mu)$ is the first term on the right-hand side of Eq. (5):

$$P \equiv f(\mu) + \frac{\gamma}{V} E. \tag{9}$$

By choosing a sequence of $V_2 < V_1$ and calculating E_2 from Eq. (8), the double-shock Hugoniot $P_2(V_2,E_2,V_1,E_1)$ is calculated from Eq. (9). To transform to $P - u_p$ space for shock-impedance matching, u_{p2} is obtained by combining Eqs. (1a) and (1b),

$$u_{p2} = u_{p1} - [\,(P_2 - P_1)/(V_1 - V_2)\,]^{1/2}. \tag{10}$$

The double-shock state in nitrogen is then the state $P_2(u_{p2})$ where the window or anvil Hugoniot $P_{An}(u_p)$ intersects $P_2(u_{p2})$:

$$P_2(u_{p2}) = P_{An}(u_{p2}) = \rho_{0An}\, u_{sAn}\, u_{p2} \tag{11}$$

and

$$u_{sAn} = C_{An} + S_{An} u_{p2}. \tag{12}$$

This method is valid provided the second-shock volume does not approach close to or become less than the limiting volume compression of the principal Hugoniot. When this occurs the reference curve assumed for the Grüneisen equation of state is no longer valid and neither is Eq. (5). For nitrogen Eq. (5) is valid for $V > 10$ cm^3/mol. The uncertain-

TABLE VI. Shock temperatures and emissivities for single-shocked liquid nitrogen. Initial nitrogen density was 0.808 g/cm^3. Pressures, densities, shock velocities, and mass velocities were obtained by shock-impedance matching. Molar volume is calculated per mole of N_2.

Shot	Impactor	u_I (km/s)	u_{p1} (km/s)	u_s (km/s)	P_1 (GPa)[a]	V_1 (cm^3/mol)	T_1 (K)	Emissivity
LNT06	Al	4.485	3.53	6.34	18.1 ± 0.5	15.34 ± 0.04	4 300 ± 200	0.12
LNT01	Al	5.550	4.29	7.46	25.8 ± 0.5	14.75 ± 0.07	5 700 ± 200	1.00 ± 0.15
LNT08	Al	6.085	4.67	7.93	29.9 ± 0.5	14.26 ± 0.08	7 300 ± 250	0.41 ± 0.06
LNT07	Al	6.735	5.14	8.44	35.0 ± 0.4	13.55 ± 0.08	8 400 ± 300	0.65 ± 0.10
LNT02	Al	6.860	5.23	8.52	36.0 ± 0.4	13.41 ± 0.08	8 750 ± 300	1.00 ± 0.15
LNT12	Ta	5.490	6.19	9.40	47.0 ± 0.5	11.83 ± 0.08	8 900 ± 600	1.00 ± 0.15
LNT04	Cu	6.510	6.65	9.79	52.6 ± 0.5	11.13 ± 0.08	11 100 ± 800	0.80 ± 0.12
LNT03	Ta	6.470	7.25	10.31	60.4 ± 0.7	10.31 ± 0.07	12 000 ± 850	0.95 ± 0.14
LNT09	Ta	7.716	8.55	11.73	81.1 ± 1.5	9.40 ± 0.06	14 500 ± 1000	0.58 ± 0.09

[a] 1 GPa = 10 kbar.

ties in the double-shock pressures and volumes were assumed comparable to those of the double-shock EOS experiments.

For volumes at which the Grüneisen model is invalid, Ross' theory for the double-shock curves of nitrogen were shock-impedance matched with the Hugoniots of the Al_2O_3 or LiF windows to obtain the second-shock states. In practice the experimentally normalized Grüneisen equation of state was used for experiments with a first-shock pressure of 36 GPa or less. Theory was used for the higher-pressure experiments.

Thermal conduction across the interface between hot double-shocked nitrogen and a cool Al_2O_3 window during the time resolution of the experiment has a negligible effect on the optical emission and measured shock temperature, as discussed in the Appendix.

C. Results

Shock-temperature data for first-shock states are listed in Table VI. Double-shock temperatures derived from experiments with $P_1 \leqslant 47$ GPa are listed in Table VII.[45] Some of the values in Tables VI and VII differ somewhat from previous values.[21] The values presented here are our best ones. Single- and double-shock temperatures are plotted vs molar volume in Fig. 8, which shows that temperatures achieved by double shock to a given volume are smaller than the single-shock temperature at the same volume.

IV. ELECTRICAL CONDUCTIVITY MEASUREMENTS

A. Experiments

Electrical conductivities of shock-compressed liquid nitrogen were measured by inserting two thin metal-foil electrodes into the liquid specimen. That is, the window assembly in Fig. 6 is replaced by a dielectric insert with two metal-foil electrodes. The method has been described previously.[46–48] Briefly, two 0.05 mm thin parallel foils 1 mm wide centered on axis and separated by 1 mm extend 1 mm into the liquid specimen parallel to the shock direction. A shock wave typically traverses the 1 mm length of the electrodes in 100 ns. At highest pressures where the specimen conductivity is highest, low-resistance Cu foils were used; at lowest pressures less-delicate steel foils were used. Two electrical shorting pins were positioned in the liquid on an 18 mm diameter and were used to trigger the electronic diagnostic system. Impactor plate, Al wall, and specimen thickness were 3–4, 2–3, and 4–5 mm, respectively; specimen diameter was 30 mm. These dimensions and pin positions were chosen to eliminate radial edge effects at the electrodes. The KOVEC code was used to perform one-dimensional planar

TABLE VII. Double-shock temperatures and emissivities of nitrogen. First-shock states for these shots are listed in Table VI. Pressures, densities, and mass velocities were obtained by shock impedance matching. Molar volume is calculated per mole of N_2.

Shot	Anvil	u_{p2} (km/s)	P_2 (GPa)	V_2 (cm^3/mol)	T_2 (K)	Emissivity
LNT06	Al_2O_3	1.33	53.1	11.4	6500 ± 500	0.35 ± 0.05
LNT01	Al_2O_3	1.77	73.9	11.1	6700 ± 500	1.00 ± 0.15
LNT08	Al_2O_3	1.91	80.9	10.9	7400 ± 500	0.80 ± 0.12
LNT02	Al_2O_3	2.14	92.5	8.8	7500 ± 500	1.00 ± 0.15
LNT12	Al_2O_3	3.70	98	8.2	6900 ± 500	1.00 ± 0.15

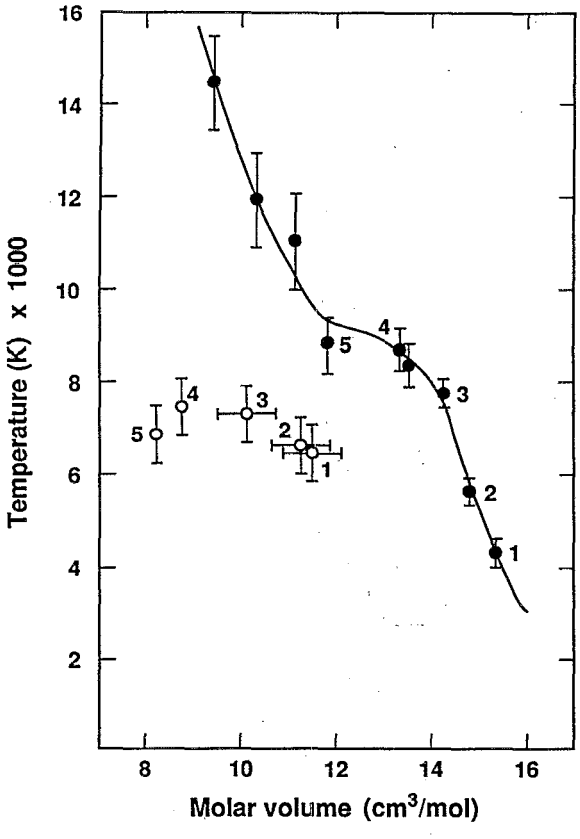

FIG. 8. Shock temperature vs molar volume of N_2. Solid circles are single-shock points. Open circles are double-shock points. Numbers show corresponding first- and second-shock points.

simulations to demonstrate that a longitudinal pressure release wave did not affect the measurements.

A constant-voltage circuit was used for measuring specimen resistances of 10 Ω or greater; a constant-current circuit was used for lower resistances. Initially liquid N_2 is an insulator. As the shock wave sweeps out an ever wider conducting area between the electrodes, current flow increases with time. The time history of the voltage is recorded on fast-sweep (50 or 100 ns/cm) Tektronix[43] 7903 oscilloscopes. For constant-voltage experiments oscilloscope deflection is calibrated prior to the shock experiment by connecting precision resistors and a low-resistance fast-closure switch to the electrodes to simulate shock-induced conduction. For constant-current experiments a precision resistor is connected in parallel with the electrodes and a current is established prior to shock arrival. The voltage history is measured across the parallel combination of the precision shunt resistor and the specimen cell. To eliminate problems with ground loops and a shifting electrical ground during gun firing, the electrodes and trigger pins were electrically isolated from the gun target chamber and electrode voltage was measured in differential mode. The geometrical factor of the cell, which relates resistivity to resistance, is calibrated prior to the shock experiment by using electrolytic solutions of known conductivity. This pulsed technique can measure conductivities in the range 10^{-5}–10^{2} $(\Omega\ \mathrm{cm})^{-1}$. For 10 ns resolution time and specimen conductivity above 10^{2} $(\Omega\ \mathrm{cm})^{-1}$ this two-probe method is compromized by high contact and circuit resistances and by long (>10 ns) flux diffusion times in the specimen.

Data were measured for singly shocked specimens. The shock pressure, volume, and internal energy of each specimen were determined by shock-impedance matching, as for the shock-temperature experiments. The shock temperature of the specimen was obtained by interpolation of the shock-temperature vs pressure data.

B. Results

Results for the electrical conductivity of shock-compressed nitrogen are given in Table VIII. The single-shock pressures and relative volumes in this table were calculated using the shock-impedance matching method described previously.[5] Uncertainties of the conductivities caused by uncertainties in the measured preshot cell constants and by the quality of the oscillograms are about 20%. This conductivity data was plotted previously vs shock pressure.[2]

TABLE VIII. Electrical conductivities of shock-compressed liquid nitrogen.

Shot	Impactor	u_I (km/s)	T_0 (K)	ρ_0 (g/cm³)	V/V_0	P (GPa)	σ $(\Omega\ \mathrm{cm})^{-1}$
NC-3	Al	7.514	77.4	0.808	0.366 ± 0.002	41.5 ± 0.5	8 ± 1
NC-6	Al	4.907	77.1	0.810	0.442 ± 0.001	21.2 ± 0.3	0.04 ± 0.004
NC-8	Al	6.586	77.3	0.809	0.394 ± 0.002	33.8 ± 0.4	2.4 ± 0.3
NC-9	Al	5.660	77.2	0.809	0.420 ± 0.001	26.6 ± 0.4	0.1 ± 0.02
NC-10	Al	4.626	77.6	0.807	0.444 ± 0.001	19.1 ± 0.3	1.5×10^{-3} $\pm 2\times10^{-4}$
NC-11	Ta	6.539	76.2	0.813	0.297 ± 0.003	61.6 ± 0.9	47 ± 6

V. DISCUSSION

The ensemble of experimental data presented here provide strong evidence for a phase transition in dense, high-temperature fluid nitrogen. For reasons summarized and referenced in Sec. I the transition is molecular dissociation to the atomic state. The transition is continuous in nature and driven by the increase in internal energy (up to 1 MJ/mol N_2), temperature, and density under shock compression. The plot of average Grüneisen parameter vs molar volume in Fig. 4 shows the onset of the transition is in a relatively narrow range of volume near 11 cm^3/mol N_2, corresponding to 2.7 times the initial density, and 7000 K. Average heat capacities have also been calculated,[21] since both temperatures and internal energies are available from the experiments. The values are relatively large, 6–9 R/mol N_2, also indicative of a phase transition. Of course, obtaining heat capacities from the data is complicated by the fact that the number of particles is not constant, due to dissociation, for single-shock and double-shock states at the same volume. For simplicity specific quantities have been converted to molar quantities throughout this work using the gram molecular weight of N_2.

The electrical conductivity data have been discussed previously.[2,48] Briefly, electrons are probably the dominant carriers by virtue of their high mobility relative to ions. The high densities and temperatures indicate that the electron mean free path is very short and relatively constant, of the order of a molecular diameter, over the range of the data.

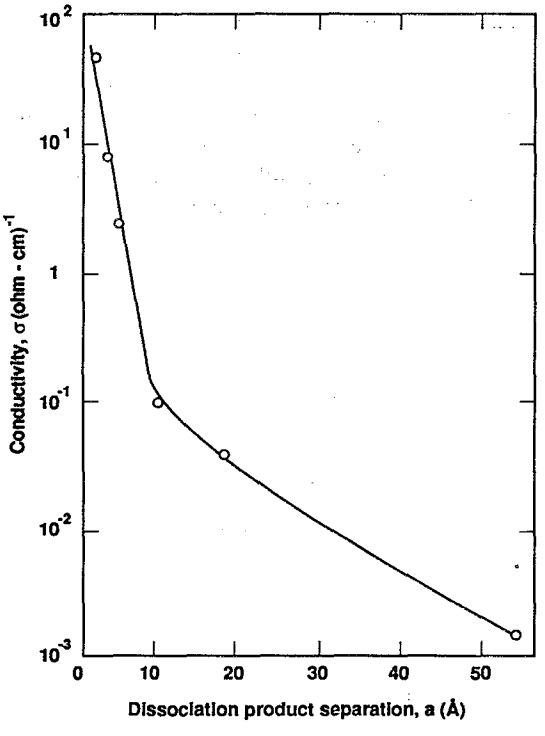

FIG. 9. Electrical conductivity of shock-compressed liquid nitrogen vs calculated dissociation product separation.

The rapid increase in conductivity with shock pressure is thus caused by a rapid increase in carrier concentration. Below the onset of the dissociative transition at 30 GPa and 7000 K electrons are ionized primarily from N_2 molecules. At higher shock pressures and temperatures, at which the dissociation fraction increases substantially, carriers are ionized primarily from N atoms. At 60 GPa about 50% of the N_2 molecules are dissociated with about 1 conduction electron per 100 original N_2 molecules.

The conductivity data can also be discussed[48] in terms of the model of electronic transport in disordered systems, as applied to shock-compressed liquid oxygen.[47] This model requires a significant degree of molecular dissociation and also that the dissociation product behave similarly to other elements in the group V column of the Periodic Table. A mean interatomic separation a between the monatomic species was calculated as for oxygen[47] using Ross' calculated dissociation fraction for nitrogen.[20] The logarithm of conductivity is plotted as a function of this interatomic separation a in Fig. 9. This plot shows features that are qualitatively similar to those observed in liquid metal systems above the critical point.[49,50] Electrical conduction for these dense, hot, disordered systems have been described in terms of thermally activated hopping and percolation for the higher pressures (smaller a's) and thermal activation of carriers across a pseudogap for lower pressures (larger a's).[51] Our results appear to be rapidly approaching Mott's value of 300 $(\Omega\ \text{cm})^{-1}$ for minimum metallic conductivity.

ACKNOWLEDGMENTS

We thank P. C. McCandless, D. L. Ravizza, R. E. Neatherland, and G. K. Governo for fabricating the cryogenic target holders, J. I. Miller, W. F. Brocious, and J. Chmielewski for fabricating the projectiles, and K. C. Pederson, R. F. Schuldheisz, C. D. Wozynski, and D. E. Bakker for firing and maintaining the two-stage light-gas gun. This work was performed under the auspices of the U.S. Department of Energy by the Lawrence Livermore National Laboratory under Contract No. W-7405-ENG-48, with partial support from the U.S. National Aeronautics and Space Administration under Grant No. W 16.180.

APPENDIX

1. Thermal conduction at the nitrogen–Al_2O_3 interface

The measured double-shock temperatures of nitrogen are about 7000 K (Table VII) and the calculated shock temperatures of the Al_2O_3 windows are about an order of magnitude smaller. The reflection of the incident shock in nitrogen off an Al_2O_3 window/anvil establishes this $\sim$7000 K temperature discontinuity at the interface instantly, that is, on a nanosecond time scale. The large temperature discontinuity will cause heat to flow by thermal conduction from the nitrogen into the Al_2O_3. The question then is what is the effect of interfacial thermal conduction and nitrogen cooling on the optical emission and, thus, on the double-shock temperature of nitrogen. In order to address this issue, the depth of cooling at the interface and the optical skin depth of dou-

ble-shocked nitrogen are estimated and compared here. The crucial time interval is the time resolution of the optical detection system, about 10 ns. This is the time required for recording the change in optical intensity when the shock wave in nitrogen reflects off the Al_2O_3. Also of interest is the effect of interfacial cooling during the lifetime of the experiment, about 100 ns.

Since shock velocities are large compared to thermal diffusion velocities, the heat-flow calculation can be performed decoupled from the hydrodynamics. That is, nitrogen at the thermodynamic conditions of the double-shock state can be considered to be in static contact with Al_2O_3 at the thermodynamic conditions of its single-shock state. The cooling at the interface was estimated by evaluating the solution of the initial value problem for heat flow between two different semi-infinite media, each initially at a different uniform temperature. The solution for the temperature T_N in the nitrogen is[52]

$$T_N = A_N[1 + B_N \operatorname{erf}(y_N)] + T_{0A}, \tag{A1}$$

where

$$A_N = \frac{K_N k_N^{-1/2}(T_{0N} - T_{0A})}{K_N k_N^{-1/2} + K_A k_A^{-1/2}}, \tag{A2}$$

$$B_N = \frac{K_A k_A^{-1/2}}{K_N k_N^{-1/2}}, \tag{A3}$$

$$y_N = \frac{x}{2(k_N t)^{1/2}}, \tag{A4}$$

$$\operatorname{erf}(y) = \frac{2}{\sqrt{\pi}} \int_0^y \exp(-z^2)dz, \tag{A5}$$

and T_{0N} and T_{0A} are the initial temperatures of nitrogen and Al_2O_3, K_N and K_A are the constant thermal conductivities of nitrogen and Al_2O_3, k_N and k_A are the constant thermal diffusivities of nitrogen and Al_2O_3. Distance x is measured positively into the nitrogen from the interface at $x = 0$.

The temperature T_A in Al_2O_3 is

$$T_A = A_N[1 - \operatorname{erf}(y_A)] + T_{0A} \tag{A6}$$

and

$$y_A = \frac{|x|}{2(k_A t)^{1/2}}. \tag{A7}$$

The initial nitrogen temperature is taken to be 7700 K (Table VII). Since Al_2O_3 is a stiff material, its thermal transport properties are determined primarily by its shock temperature. At 100 GPa the calculated shock temperature of Al_2O_3 is 960 K for an initial specimen temperature of 300 K.[53] If the specimen is initially at 77 K, the shock temperature of Al_2O_3 would be 700 K or less for pressures below 100 GPa. The initial Al_2O_3 temperature is taken to be 700 K.

The thermal conductivity of nitrogen is estimated from the kinetic theory result

$$K = \tfrac{1}{3}Cu\lambda, \tag{A8}$$

where K is thermal conductivity, C is the heat capacity per unit volume, u is the speed of sound, and λ is the mean free path of the carriers of thermal energy. Since the largest electrical conductivity measured for shocked nitrogen is a factor of 10^4 smaller than that of a good metal, we assume that nitrogen molecules and atoms are the principal carriers of thermal energy. For a heat capacity[21] of 6 R/mol of N_2 at 3.2 g/cm^3, $u = 6$ km/s (as measured here at 53 GPa shock pressure), and $\lambda = 3$ Å (a molecular diameter), $K_N = 0.034\ \mathrm{J\ K^{-1}\ cm^{-1}\ s^{-1}}$. Thermal diffusivity is

$$k = K/C = \tfrac{1}{3}u\lambda, \tag{A9}$$

and thus $k_N = 0.006\ \mathrm{cm^2\ s^{-1}}$. For Al_2O_3 at 700 K,[54] $K_A = 0.1\ \mathrm{J\ K^{-1}\ cm^{-1}\ s^{-1}}$ and $k_A = 0.02\ \mathrm{cm^2\ s^{-1}}$. The calculated spatial profile of temperature near the interface 10 and 100 ns after shock reflection are plotted in Fig. 10. A depth of only 0.2 μm of nitrogen is cooled at all by thermal diffusion into Al_2O_3 during the 10 ns time resolution of the optical detection system. A depth of about 0.4 μm of Al_2O_3 is heated into the range 900–3700 K.

The velocity with which the cooling front diffuses into the nitrogen can be calculated with Eq. (A1). When $y_N = 1$, $T_N \simeq 0.9T_{0N}$. Thus, the position x_c of a 10% cooling of the initial temperature of nitrogen is given by $x_c = 2(k_N t)^{1/2}$. At $t = 10$ ns, $v_c = dx_c/dt = 7\ \mu\mathrm{m}/\mu\mathrm{s}$, a factor of 10^3 smaller than typical shock velocities. After 500 ns, $x_c = 1\ \mu$m.

2. Optical depth of nitrogen

It is now shown that the thickness of interfacial cooling of nitrogen is small compared to its optical depth. The optical skin depth is derived[55] from the complex index of refraction n:

$$n^2 = 1 + \frac{\sigma/\varepsilon_0}{i\omega(1 + i\omega\tau)}, \tag{A10}$$

where σ is the electrical conductivity, τ is the electron scattering time, ω is the angular frequency of light, and ε_0 is the free-space dielectric constant. Electrical conductivity is given by

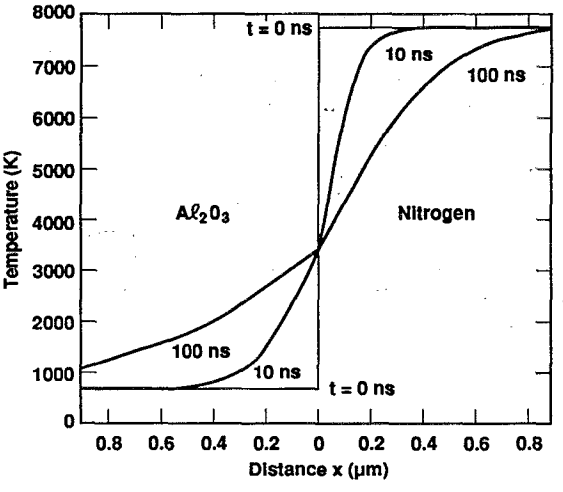

FIG. 10. Calculated temperature distribution across interface between double-shocked nitrogen and Al_2O_3 window at 10 and 100 ns after shock reflection off interface. Temperature discontinuity is 7000 K initially at $t = 0$.

$$\sigma = \frac{Ne^2\tau}{m}, \tag{A11}$$

where N is the number density of electrons, e is the electronic charge, and m is the electron mass. The skin depth δ is given by

$$\delta^{-1} = \frac{\omega n_I}{c}, \tag{A12}$$

where

$$n = n_R - in_I. \tag{A13}$$

The electronic scattering time in dense fluid nitrogen is approximated as $t = \lambda / v_{\rm th}$, where λ is the electron mean free path and $v_{\rm th}$ is the thermal velocity of the electron. λ is of order a molecular N_2 diameter, say 3 Å, in the dense hot fluid. Thermal velocity is $v_{\rm th} = (3kT/m)^{1/2}$, where k is Boltzmann's constant and T is temperature. At 7700 K, $v_{\rm th} = 6\times10^7$ cm s^{-1} and the kinetic energy is 1 eV, which is comparable to the Fermi energy estimated for this system.[20] Thus, this calculation is not very sensitive to the statistics assumed for the electrons. The scattering time is, thus, $t = 5\times10^{-16}$ s. In the optical range, say $\lambda = 500$ nm, the angular frequency is $\omega = 3.8\times10^{15}$ s^{-1}. Thus $\omega\tau = 1.9$. Since $\omega\tau \sim 1$, the skin depth must be calculated as discussed above and the usual low-frequency approximation $\omega\tau \ll 1$ for microwaves in metals cannot be used.

The electrical conductivity of nitrogen in the double-shock state has not been measured. Two limits are, therefore, considered which probably bound the actual situation. The first case is to assume that the electrical conductivity is determined primarily by temperature and is only weakly sensitive to density in the range of the experiments, 9–11 cm^3/mol of N_2. In this case the value of $\sigma = 1\ (\Omega\ {\rm cm})^{-1}$ (at 7700 K on the Hugoniot) is used. The other limit is to assume the largest value of σ which was measured, $\sigma = 50\ (\Omega\ {\rm cm})^{-1}$ (at 12 000 K and 10.4 cm^3/mol of N_2). If $\sigma = 1\ (\Omega\ {\rm cm})^{-1}$, then $n^2 = 1.00$–$6.45\times10^{-4}\ i$ and $n_I = 3.23\times10^{-4}$. At $\lambda = 500$ nm, therefore, $\delta = 240$ μm, which is very large compared to the 0.2 μm thin layer of nitrogen cooled by thermal diffusion during the time resolution of the double-shock temperature measurement. This optical depth is also large compared to the 1 μm thin layer cooled during the 500 ns lifetime of the experiment. For $\sigma = 50\ (\Omega\ {\rm cm})^{-1}$, $\delta = 5$ μm at $\lambda = 500$ nm, which is still large compared to the thin cooled layers. Also, as the interfacial layer cools, the electrical conductivity drops rapidly and the transparency of the cooled nitrogen increases. These considerations lead to the conclusion that the effect of interfacial cooling of nitrogen by thermal conduction has a negligible effect on the measured optical emission intensities and thus on the double-shock temperature during the time resolution of the optical detection system.

[1] W. J. Nellis, N. C. Holmes, A. C. Mitchell, and M. van Thiel, Phys. Rev. Lett. **53**, 1661 (1984).

[2] H. B. Radousky, W. J. Nellis, M. Ross, D. C. Hamilton, and A. C. Mitchell, Phys. Rev. Lett. **57**, 2419 (1986).

[3] V. N. Zubarev and G. S. Telegin, Dokl. Akad. Nauk SSSR **142**, 309 (1962) [Sov. Phys. Dokl. **7**, 34 (1962)].

[4] R. D. Dick, J. Chem. Phys. **52**, 6021 (1970).

[5] W. J. Nellis and A. C. Mitchell, J. Chem. Phys. **73**, 6137 (1980).

[6] G. L. Schott, M. S. Shaw, and J. D. Johnson, J. Chem. Phys. **82**, 4264 (1985).

[7] M. Ross and F. H. Ree, J. Chem. Phys. **73**, 6146 (1980).

[8] M. Voskoboinikov, M. F. Gogulya, and Yu. A. Dolgoborodov, Dokl. Akad. Nauk SSSR **246**, 579 (1979) [Sov. Phys. Dokl. **24**, 375 (1979)].

[9] B. L. Holian, J. Chem. Phys. **84**, 3138 (1986).

[10] S. C. Schmidt, D. S. Moore, and M. S. Shaw, Phys. Rev. B **35**, 493 (1987).

[11] D. S. Moore, S. C. Schmidt, M. S. Shaw, and J. D. Johnson, J. Chem. Phys. **90**, 1368 (1989).

[12] F. H. Ree and N. W. Winter, J. Chem. Phys. **73**, 322 (1980).

[13] R. LeSar and M. S. Shaw, J. Chem. Phys. **84**, 5479 (1986).

[14] M. S. Shaw, J. D. Johnson, and B. L. Holian, Phys. Rev. Lett. **50**, 1141 (1983).

[15] J. D. Johnson, M. S. Shaw, and B. L. Holian, J. Chem. Phys. **80**, 1279 (1984).

[16] M. S. Shaw, J. D. Johnson, and J. D. Ramshaw, J. Chem. Phys. **84**, 3479 (1986).

[17] R. LeSar, J. Chem. Phys. **86**, 4138 (1987).

[18] R. D. Etters, J. Belak, and R. LeSar, Phys. Rev. B **34**, 4221 (1986).

[19] M. Ross and A. K. McMahan, in *Physics of Solids under High Pressure*, edited by J. S. Schilling and R. N. Shelton (North-Holland, Amsterdam, 1981), p. 161.

[20] M. Ross, J. Chem. Phys. **86**, 7110 (1987).

[21] H. B. Radousky and M. Ross, High Press. Res. **1**, 39 (1988).

[22] D. C. Hamilton and F. H. Ree, J. Chem. Phys. **90**, 4972 (1989).

[23] G. I. Kerley and A. C. Switendick, in *Shock Waves in Condensed Matter*, edited by Y. M. Gupta (Plenum, New York, 1986), p. 95.

[24] D. A. Young, C.-S. Zha, R. Boehler, J. Yen, M. Nicol, A. S. Zinn, D. Schiferl, S. Kinkead, R. C. Hanson, and D. A. Pinnick, Phys. Rev. B **35**, 5353 (1987).

[25] A. K. McMahan and R. LeSar, Phys. Rev. Lett. **54**, 1929 (1985).

[26] R. Reichlin, D. Schiferl, S. Martin, C. Vanderborgh, and R. L. Mills, Phys. Rev. Lett. **55**, 1464 (1985).

[27] P. M. Bell, H. K. Mao, and R. J. Hemley, Physica B **139 & 140**, 16 (1986).

[28] B. Olinger, J. Chem. Phys. **80**, 1309 (1984).

[29] S. Buchsbaum, R. L. Mills, and D. J. Schiferl, J. Phys. Chem. **88**, 2522 (1984).

[30] D. Schiferl, S. Buchsbaum, and R. L. Mills, J. Phys. Chem. **89**, 2324 (1985).

[31] M. Grimsditch, Phys. Rev. B **32**, 514 (1985).

[32] A. H. Jones, W. M. Isbell, and C. J. Maiden, J. Appl. Phys. **37**, 3493 (1966).

[33] A. C. Mitchell and W. J. Nellis, Rev. Sci. Instrum. **52**, 347 (1981).

[34] W. J. Nellis, F. H. Ree, M. van Thiel, and A. C. Mitchell, J. Chem. Phys. **75**, 3055 (1981).

[35] H. M. Roder, R. D. McCarty, and V. J. Johnson, Natl. Bur. Stand. (U.S.) Tech. Note 361 (1972).

[36] A. C. Mitchell and W. J. Nellis, J. Appl. Phys. **52**, 3363 (1981).

[37] J. R. Asay, L. C. Chhabildas, G. I. Kerley, and T. G. Trucano, in *Shock Waves in Condensed Matter*, edited by Y. M. Gupta (Plenum, New York, 1986), pp. 145–149.

[38] M. L. Wilkins, Lawrence Livermore National Laboratory, UCRL-7322, Rev. 1 (1969).

[39] R. Grover (Lawrence Livermore National Laboratory, private communication, 1986).

[40] H. B. Radousky, in *Shock Waves in Condensed Matter 1987*, edited by S. C. Schmidt and N. C. Holmes (Elsevier, Amsterdam, 1988), p. 89; H. B. Radousky and A. C. Mitchell, Rev. Sci. Instrum. **60**, 3707 (1989).

[41] P. A. Urtiew, J. Appl. Phys. **45**, 3490 (1974).

[42] J. L. Wise and L. C. Chhabildas, in *Shock Waves in Condensed Matter*, edited by Y. M. Gupta (Plenum, New York, 1986), p. 441.

[43] Reference to a company or product name does not imply approval or recommendation of the product by the University of California or the U.S. Department of Energy to the exclusion of others that may be suitable.

[44] L. V. Altshuler, S. B. Kormer, M. I. Brazhnik, L. A. Vladimirov, M. P. Speranskaya, and A. I. Funtikov, J. Exptl. Theoret. Phys. (U.S.S.R.) **38**, 1061 (1960) [Sov. Phys. JETP **11**, 766 (1960)].

[45] The higher-pressure experiments did not permit derivation of double-shock temperatures. Shot LNTO4 was designed to observe the pressure release wave overtaking the first shock. Shots LNTO3 and LNTO9 pro-

duced double-shock pressures above 160 GPa where the opacity of shocked Al_2O_3 is as yet unresolved, which precludes interpretation of the emission data in terms of temperature.
[46] A. C. Mitchell and W. J. Nellis, J. Chem. Phys. **76**, 6273 (1982).
[47] D. C. Hamilton, W. J. Nellis, A. C. Mitchell, F. H. Ree, and M. van Thiel, J. Chem. Phys. **88**, 5042 (1988).
[48] D. C. Hamilton, Ph.D. Thesis, University of California, Lawrence Livermore National Laboratory report UCRL-53768, 1988.
[49] H. Hoshino, R. W. Schmutzler, W. W. Warren, and F. Hensel, Philos. Mag. **33**, 255 (1976).
[50] H. Renkert, F. Hensel, and E. U. Franck, J. Non-Cryst. Solids **4**, 180 (1970).
[51] N. F. Mott and E. A. Davis, *Electronic Processes in Non-Crystalline Materials* (Clarendon, Oxford, 1979).
[52] H. S. Carslaw and J. C. Jaeger, *Conduction of Heat in Solids* (Clarendon, Oxford, 1959), p. 88.
[53] T. J. Ahrens, W. H. Gust, and E. B. Royce, J. Appl. Phys. **39**, 4610 (1968).
[54] *Thermophysical Properties of High Temperature Solid Materials, Volume 4: Oxides and Their Solutions and Mixtures*, edited by Y. S. Touloukian (MacMillan, New York, 1967), pp. 11–20.
[55] R. P. Feynman, R. B. Leighton, and M. Sands, *The Feynman Lectures on Physics* (Addison-Wesley, Reading, Mass., 1964), Vol. II, p. 32–10.